Biointerface Research in Applied Chemistry
Open-Access Journal (ISSN: 2069-5837)

Article
Volume 15, Issue 5, 2025, 62
https://doi.org/10.33263/BRIAC155.062

Scavenging of Heavy Metal Ions (Cr^{3+}, Mn^{2+}, Co^{2+}, Ni^{2+}, Cu^{2+}, Zn^{2+}) from Water by GaN Nanomaterial: An Environmental Eco-friendly System by Molecular Modelling Approach

Fatemeh Mollaamin [1,*]

[1] Department of Biomedical Engineering, Faculty of Engineering and Architecture, Kastamonu University, Kastamonu, Turkey
* Correspondence: fmollaamin@kastamonu.edu.tr;

Received: 17.10.2024; Accepted: 19.07.2025; Published: 9.08.2025

Abstract: Removal of heavy metal cations of Cr^{3+}, Mn^{2+}, Co^{2+}, Ni^{2+}, Cu^{2+}, Zn^{2+} from simulated water due to nanomaterial-based gallium nitride nanocage ($Ga_5N_{10}Nc$) is the target of this research. $Ga_5N_{10}Nc$ was modeled in the presence of heavy metal cations (Cr^{3+}, Mn^{2+}, Co^{2+}, Ni^{2+}, Cu^{2+}, Zn^{2+}). The essence of covalent traits for these composites displays the equivalent energy and visibility of the partial density of states (PDOS) for the *p* states of nitrogen and *d* states of heavy metal ions of Cr^{3+}, Mn^{2+}, Co^{2+}, Ni^{2+}, Cu^{2+}, Zn^{2+} through water treatment. In other words, the chemical amendment twists the covalent bonding of functional groups on the backbone of the hybrid composite of gallium nitride towards a striking enhancement in the adsorption capacity parameter. In addition, the nuclear magnetic resonance (NMR) analysis suggested the substantial peaks surrounding metal ions of Cr^{3+}, Mn^{2+}, Co^{2+}, Ni^{2+}, Cu^{2+}, and Zn^{2+} on the hybrid composite of gallium nitride during ion deletion from water. On the other hand, the selectivity of metal ion adsorption by a byhybrid composite of gallium nitride has been authorized as: Ni^{2+}>>> Cu^{2+} > Co^{2+}> Mn^{2+} > Cr^{3+} >> Zn^{2+}. In this research, it is suggested that heavy metal ions adsorbed can be applied to amplify the optoelectronic properties of gallium nitride, which can be used to develop photoelectric instruments for water purification.

Keywords: $Ga_5N_{10}Nc$; water contaminant; molecular modeling; nanomaterial; DFT; adsorption; heavy metal remediation.

1. Introduction

The quantity and quality of the chemical atoms in surface waters are impacted by the geochemical combination of environment, soil use, changes in seasonal climate, vegetation, and the atmospheric conditions [1–6].

These days, atmospheric contaminations caused by toxic organic compounds and hazardous heavy metals, with their persistence, are a serious obstacle all over the world [7,8]. For instance, lead (Pb) is a heavy metal that exists abundantly in the environment. The improvement of the lifestyle and dependent productions enhanced the value of lead emissions and led to an explicit growth in doping in the surroundings [9,10]. Lead does not decompose in the environment, so it collects in the living cells and poses a high health hazard [11,12].

Pollution in the environment with different kinds of chromium (Cr) results from its abundant utilization in the chemical industry, production of dyes, wood protection, leather tanning, chrome coating, construction of diverse alloy materials, and numerous other uses and productions [13,14]. The supplies of drinking water in various zones consist of Cr in the +3 and +6 oxidation states [15,16]. Co and its compounds are employed in metallurgical technology, electroplating, the nuclear industry, fertilizers, and medical issues. Whenever an excess Co metal enters the human body, it is damaging [17]. In addition, it is supposed that consumption of Cu at concentrations higher than the prescribed amount may cause serious health diseases such as gastrointestinal disorders, central nervous maladies, mucosal pain, Wilson's problems, harm to the kidney and liver, etc. [18,19]. Moreover, the potency of pristine and functionalized biochars for adsorbing and removing nickel in water and soil has not been systematically investigated [20,21]. Newly, an overview of the potential of magnetite nanoparticles and their composites to treat polluted water and scavenge unpleasant contaminants has been presented [22].

The researchers have investigated the priority and selectivity of metal grabbing on the basis of the nature of surfactant in foam separation [23–25]. Generally, pursuant to Hoffmeister's series, it was announced that the first group metals with lower atomic numbers may be precipitated with carboxylic acid (R-COOH) in watery solutions [26–28].

The gallium nitride (GaN) molecule is one of the most explored of the third group semiconductors containing nitrogen, which are employed in various applications such as detector tools, optoelectronic and electronic instruments [29–32]. Regarding the important electronic attributes of GaN, it can be a suitable sample for gas detection [33–35]. In addition, density function theory (DFT) can be applied to investigate the mechanisms of complexes and adsorption reactions [36–39]. On this basis, the application of DFT in the adsorption reaction system is summarized in this paper.

Compared to the past semiconductor substances, 3D-GaN is a broadband gap semiconductor system [40]. Therefore, it can empower instrument operation at high frequency/voltage, or temperature, and indicates high luminous yield, proper thermal conduction, high temperature persistence, stability to acids and alkalis, and anti-radiation attributes [41]. Adsorption of Elements on the solid surface might interact indirectly through elastic distortion of the substrate or electron scattering with a long-range atomic interaction adjusted by the substrate, playing a significant role in the self-assembly atomic shape. Since alkali metal elements might lightly miss electrons, their adsorption on the semiconducting nanomaterials might change them to n-type, which will in turn decrease their effective action and alter their optoelectronic attributes [42]. Recently, many researchers have announced verdicts on the optoelectronic attributes of alkali-metal-adsorbed two-dimensional materials [43–53]. The alkali-metal atoms adsorbing on graphene [43,44] and g-GaN [54], using a first-principles approach, have been studied, and it has been discovered that the optoelectronic properties of graphene and g-GaN are improved by the adsorption of alkali metals.

The density of $Ga_5N_{10}Nc$ material is low. Therefore, it is envisaged to address the limitations of contaminants and overcome the weak adsorption, quick compression, and secondary pollution in the modification technology. As a matter of fact, the target of this research is to trap the cations of Cr^{3+}, Mn^{2+}, Co^{2+}, Ni^{2+}, Cu^{2+}, and Zn^{2+} in the water phase by theoretical methods.

2. Materials and Methods

2.1. Encapsulation of heavy metals in $Ga_5N_{10}Nc$.

The purpose of this work is to grab heavy metal cations from water by using $Ga_5N_{10}Nc$. The intention is to remove Cr^{3+}, Mn^{2+}, Co^{2+}, Ni^{2+}, Cu^{2+}, Zn^{2+} from the water phase, consisting of a series of heavy metal cations. The water phase surrounds the heavy metal cations and the $Ga_5N_{10}Nc$ (Figure 1). $Ga_5N_{10}Nc$ was modeled in the presence of heavy metal cations (Cr^{3+}, Mn^{2+}, Co^{2+}, Ni^{2+}, Cu^{2+}, Zn^{2+}). Sample characterization was performed by CAM–B3LYP/EPR–3, LANL2DZ level of theory.

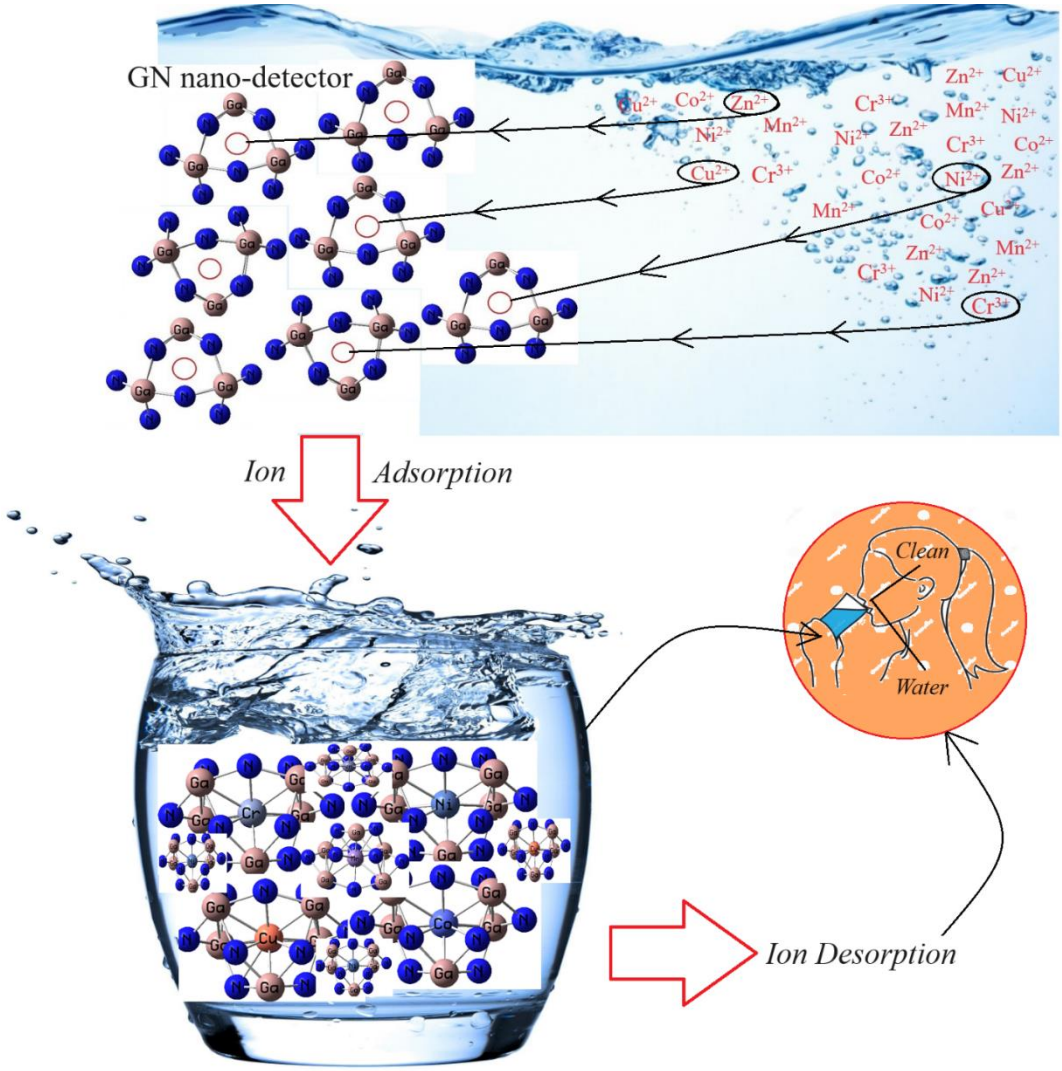

Figure 1. The mechanism of encapsulation of the ions (Cr^{3+}, Mn^{2+}, Co^{2+}, Ni^{2+}, Cu^{2+}, Zn^{2+}) in water via $Ga_5N_{10}Nc$ and formation of $Cr^{3+}\rightarrow Ga_5N_{10}Nc$, $Mn^{2+}\rightarrow Ga_5N_{10}Nc$, $Co^{2+}\rightarrow Ga_5N_{10}Nc$, $Ni^{2+}\rightarrow Ga_5N_{10}Nc$, $Cu^{2+}\rightarrow Ga_5N_{10}Nc$, and $Zn^{2+}\rightarrow Ga_5N_{10}Nc$ complexes.

The heavy metal cations were successfully incorporated in the center of $Ga_5N_{10}Nc$ towards formation of $Cr^{3+}\rightarrow Ga_5N_{10}Nc$, $Mn^{2+}\rightarrow Ga_5N_{10}Nc$, $Co^{2+}\rightarrow Ga_5N_{10}Nc$, $Ni^{2+}\rightarrow Ga_5N_{10}Nc$, $Cu^{2+}\rightarrow Ga_5N_{10}Nc$, and $Zn^{2+}\rightarrow Ga_5N_{10}Nc$ complexes (Figure 1), and the charge distribution of these complexes has been computed owing to the parameter of Bader charge evaluation [55]. Irrespective of the element, the $Ga_5N_{10}Nc$ becomes bigger for embedding the metal elements. The polarizable continuum model (PCM) using the integral equation formalism variant (IEFPCM) is the default SCRF method [56] using Gaussian 16 revision C.01 software [57]. This method creates the solute cavity via a set of overlapping spheres [58].

2.2. Application of DFT approach.

The computational work in this research article was performed owing to the perceptual DFT applying the projector– augmented–wave (PAW) technique [59]. The Perdew–Burke–Ernzerhof (PBE) functional under the generalized gradient approximation (GGA) was employed as the exchange-correlation functional [60]. The non-empirical PBE functional is diagnosed to concede stringent crystal nominations [61]. Popularly, when GGA functionals are missing, local density functionals also cease. Regarding the thermal conductance measured to local density functionals, PBE does not append compounds, and thus, the force constants of interatomic interactions are not so pliable. In fact, the lattice thermal conductance is wholly uniform if employing GGA functionals or local density [62].

The functions of Hohenberg-Kohn (HK) theory have rigidly caused the electronic density to be permissible as a fundamental variable in structure/electronic computations. On the other hand, the development of the applied DFT methodology only grew notable after W. Kohn and L. J. Sham released their reputable series of equations, which are introduced as Kohn-Sham (KS) equations [63,64].

Considering the electronic density within the KS image suggests a remarkable reduction in quantum computing. Thus, the KS methodology lightens the route for pursuing the systems that couldn't be discussed by conventional Ab Initio methodologies. Kohn and Sham" introduces the solution that brings up the mono-electronic orbitals to account for the kinetic energy in a modest and relatively exact manner, by finding a residual modification that might be computed apart. So, one starts with a reference model of *M* with non-interactive electrons related to the external potential v_s accompanying Hamiltonian factor [63,64]:

$$\hat{H}_s = -\sum_i^M \frac{1}{2}\overline{\nabla}_i^2 + \sum_i^M v_s(\vec{r}_i) = \sum_i^M \hat{h}_s\,;\quad \hat{h}_s = -\frac{1}{2}\overline{\nabla}_i^2 + v_s(\vec{r}_i) \qquad (1)$$

By representing the single-particle orbitals ψ_i all electronic densities admissible for the group of "non-interacting" electrons are observed in the equation (2):

$$\rho(\vec{r}) = \sum_i^M |\psi_i(\vec{r})|^2 \qquad (2)$$

Eventually, the total energy might be measured by the KS method due to equation (3):

$$E[\rho] = \sum_i^M n_i \langle \psi_i \left| -\frac{1}{2}\overline{\nabla}^2 + v_{ext}(\vec{r}) + \frac{1}{2}\int \frac{\rho(\vec{r}')}{|\vec{r}-\vec{r}'|}\,\mathrm{d}\vec{r}' \right| \psi_i \rangle + E_{xc}[\rho] + \frac{1}{2}\sum_\beta^N \sum_{\alpha\neq\beta}^N \frac{Z_\alpha Z_\beta}{|\vec{R}_\alpha - \vec{R}_\beta|} \qquad (3)$$

Thus, the precise exchange energy functional is described by the «Kohn–Sham orbitals» in lieu of the density, which is cited as the indirect density functional. So, the present research employed the penetration of the hybrid functional of the 3-parameter basis set of B3LYP «Becke, Lee, Yang, Parr» within the conception of DFT upon theoretical computations [65,66]. The popular B3LYP «Becke/three-parameter/Lee–Yang–Parr» and exchange-correlation functional becomes based on equation (4) [67–70]:

$$E_{\mathrm{XC}}^{\mathrm{B3LYP}} = (1-\alpha)E_{\mathrm{x}}^{\mathrm{LSDA}} + \alpha E_{\mathrm{x}}^{\mathrm{HF}} + b\Delta E_{\mathrm{x}}^{\mathrm{B}} + (1-c)E_{\mathrm{c}}^{\mathrm{LSDA}} + cE_{\mathrm{c}}^{\mathrm{LYP}} \qquad (4)$$

$\alpha = 0.20, b = 0.72, c = 0.81$ shows the GGA. In this article, the rigid PES using DFT computations was carried out using Gaussian 16 revision C.01 software [57]. The GJF file of geometry coordination for encapsulation of the metal cations including Cr^{3+}, Mn^{2+}, Co^{2+}, Ni^{2+},

Cu^{2+}, Zn^{2+} in water by the $Ga_5N_{10}Nc$ was prepared due to GaussView 6.1 [71] via the solid model and coordination template of which an interval line was placed accompanying the LANL2DZ level of theory to discern quantum chemical properties for metal cations (Figure 2).

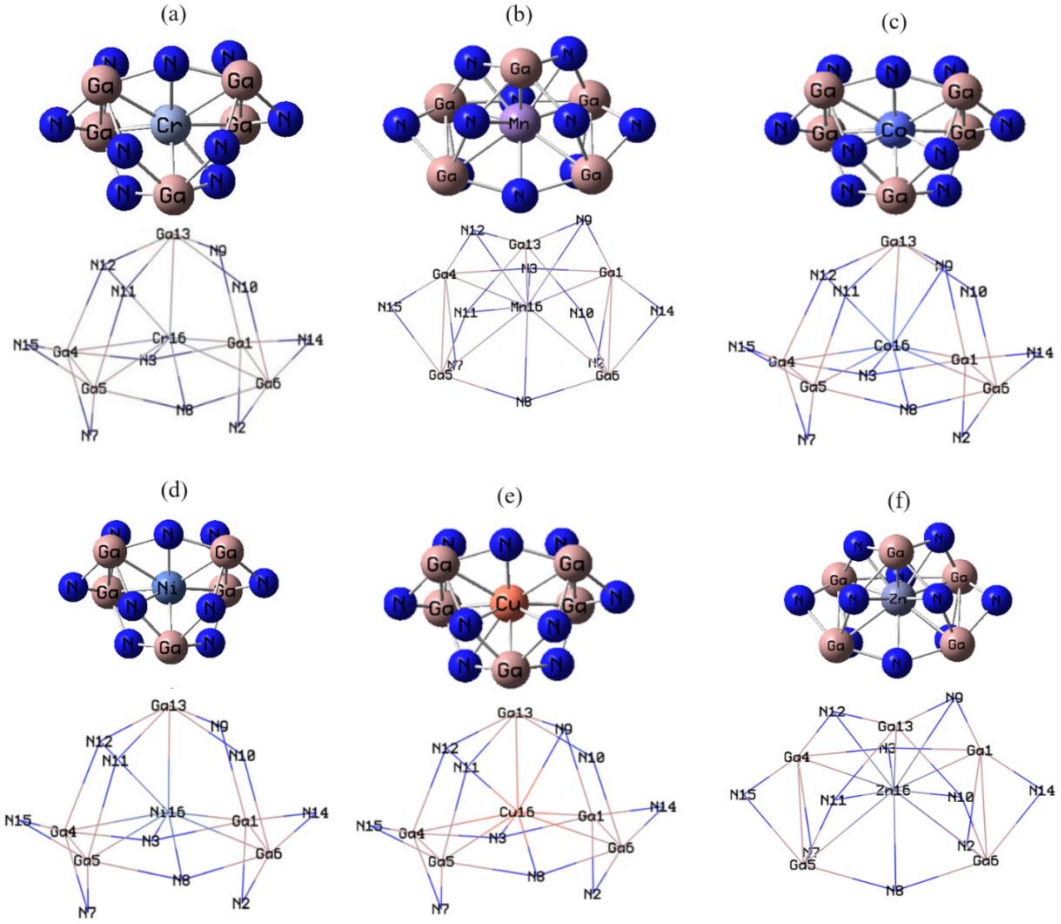

Figure 2. Optimized complexes of **(a)** Cr^{3+}→ $Ga_5N_{10}Nc$; **(b)** Mn^{2+}→ $Ga_5N_{10}Nc$; **(c)** Co^{2+}→ $Ga_5N_{10}Nc$; **(d)** Ni^{2+}→ $Ga_5N_{10}Nc$; **(e)** Cu^{2+}→ $Ga_5N_{10}Nc$; **(f)** Zn^{2+}→ $Ga_5N_{10}Nc$ using CAM–B3LYP/EPR–3, LANL2DZ.

3. Results and Discussion

The data has evaluated the efficiency of $Ga_5N_{10}Nc$ for heavy metal cations encapsulation. In fact, it can be remarked that the chemical essence of the binding in the metal cations with gallium and nitrogen elements through the equilibrium distribution of metal cations, $Ga_5N_{10}Nc$, and a monolayer attribute.

3.1. Insight into nuclear quadrupole resonance (NQR).

The trapping of first and second main group metal cations, including Cr^{3+}, Mn^{2+}, Co^{2+}, Ni^{2+}, Cu^{2+}, Zn^{2+}, in the $Ga_5N_{10}Nc$ by NQR calculation was carried out.

As the electric field gradient (EFG) at the placement of the nucleus in heavy metal cations including Cr^{3+}, Mn^{2+}, Co^{2+}, Ni^{2+}, Cu^{2+}, Zn^{2+} is assigned by the valence electrons distorted in the net affiliation with intimate nuclei of $Ga_5N_{10}Nc$ through trapping of metal cations, the «NQR» frequency at which intermediates happen is sole for Ions→ $Ga_5N_{10}Nc$ complexes (Ions = Cr^{3+}, Mn^{2+}, Co^{2+}, Ni^{2+}, Cu^{2+}, Zn^{2+}) (Table 1). NQR is an upstanding skeleton of the action/reaction of the quadrupole moment with the EFG that is brought forward by the electronic environment of its surroundings. Thus, the NQR transmission frequencies are

symmetric to the electric quadrupole moment of the nucleus and a deliberation of the rigidity of the residential EFG amount [72,73]. The approach of «NQR» is related to the multipole expansion in Cartesian coordinates as in equation (5):

$$V(r) = V(0) + \left[\left(\frac{\partial V}{\partial x_i}\right)\Big|_0 . x_i\right] + \frac{1}{2}\left[\left(\frac{\partial^2 V}{\partial x_i x_j}\right)\Big|_0 . x_i x_j\right] \quad (5)$$

After that, a simplification of the equation (5), it can be observed lonely the second derivatives related to the identical variable for the potential energy parameter [70,71]:

$$U = -\frac{1}{2}\int_{\mathcal{D}} d^3\, r\, \rho_r \left[\left(\frac{\partial^2 V}{\partial x_i^2}\right)\Big|_0 . x_i^2\right] = -\frac{1}{2}\int_{\mathcal{D}} d^3\, r\, \rho_r \left[\left(\frac{\partial E_i}{\partial x_i}\right)\Big|_0 . x_i^2\right] = -\frac{1}{2}\left(\frac{\partial E_i}{\partial x_i}\right)\Big|_0 . \int_{\mathcal{D}} d^3\, r\, [\rho(r) . x_i^2] \quad (6)$$

Two factors are discussed, which are extracted from NQR values: the quadrupole coupling constant, χ, and the asymmetry parameter of the EFG tensor, η:

$$\chi = {e^2 Q q_{zz}}/{h} \quad (7)$$

$$\eta = {q_{xx} - q_{yy}}/{q_{zz}} \quad (8)$$

Where q_{ii} are the ingredients of the «EFG» tensor at the quadrupole nucleus resolved in the «EFG» principal axes system, Q is the NQR, e is the proton charge, and h is Planck's constant parameter [74,75].

In the research work, the electric potential as the quantity of applied energy through carrying over the electric charge from one position to another position in the essence of electric field was evaluated for Cr^{3+}→ $Ga_5N_{10}Nc$, Mn^{2+}→ $Ga_5N_{10}Nc$, Co^{2+}→ $Ga_5N_{10}Nc$, Ni^{2+}→ $Ga_5N_{10}Nc$, Cu^{2+}→ $Ga_5N_{10}Nc$, and Zn^{2+}→ $Ga_5N_{10}Nc$ materials accompanying CAM–B3LYP/EPR–3, LANL2DZ keywords (Table 1).

Table 1. The electric potential (a.u.) and Bader charge (e) through NQR calculation for Cr^{3+}→ $Ga_5N_{10}Nc$, Mn^{2+}→ $Ga_5N_{10}Nc$, Co^{2+}→ $Ga_5N_{10}Nc$, Ni^{2+}→ $Ga_5N_{10}Nc$, Cu^{2+}→ $Ga_5N_{10}Nc$, and Zn^{2+}→ $Ga_5N_{10}Nc$ complexes using CAM-B3LYP/EPR–3, LANL2DZ calculation.

Cr^{3+}→ $Ga_5N_{10}Nc$			**Mn^{2+}→ $Ga_5N_{10}Nc$**			**Co^{2+}→ $Ga_5N_{10}Nc$**		
Atom	**Q**	**E_p**	**Atom**	**Q**	**E_p**	**Atom**	**Q**	**E_p**
Ga1	0.6782	–1.2180	Ga1	0.6765	–1.2161	Ga1	0.7494	–1.2158
N2	–0.4114	–18.4112	N2	–0.3606	–18.4000	N2	–0.3335	–18.3919
N3	–0.4288	–18.4032	N3	–0.5082	–18.4080	N3	–0.5045	–18.4052
Ga4	0.6497	–1.2090	Ga4	0.6643	–1.2143	Ga4	0.7456	–1.2151
Ga5	0.6877	–1.2091	Ga5	0.7000	–1.2144	Ga5	0.7730	–1.2182
Ga6	0.6931	–1.2175	Ga6	0.6869	–1.2141	Ga6	0.7401	–1.2164
N7	–0.4055	–18.4017	N7	–0.3593	–18.4007	N7	–0.3522	–18.4087
N8	–0.4419	–18.4039	N8	–0.5168	–18.4068	N8	–0.5119	–18.3991
N9	–0.3624	–18.409	N9	–0.3552	–18.3870	N9	–0.3419	–18.3801
N10	–0.3728	–18.406	N10	–0.3403	–18.3790	N10	–0.3692	–18.4028
N11	–0.3470	–18.3904	N11	–0.3413	–18.3781	N11	–0.3692	–18.3949
N12	–0.3936	–18.411	N12	–0.3672	–18.3878	N12	–0.3578	–18.3784
Ga13	0.6603	–1.2002	Ga13	0.6445	–1.185	Ga13	0.7533	–1.1899
N14	–0.4222	–18.4188	N14	–0.4414	–18.4162	N14	–0.4390	–18.4178
N15	–0.3872	–18.3997	N15	–0.4502	–18.4134	N15	–0.4489	–18.4104
Cr^{3+}16	0.6038	–22.5967	Mn^{2+}16	0.6686	–26.6124	Co^{2+}16	0.2667	–21.1214
Ni^{2+}→ $Ga_5N_{10}Nc$			**Cu^{2+}→ $Ga_5N_{10}Nc$**			**Zn^{2+}→ $Ga_5N_{10}Nc$**		

Atom	Q	E_p	Atom	Q	E_p	Atom	Q	E_p
Ga1	0.7816	–1.1951	Ga1	0.7829	–1.2117	Ga1	0.7366	–1.2076
N2	–0.3275	–18.3984	N2	–0.3407	–18.399	N2	–0.4119	–18.4183
N3	–0.5343	–18.4074	N3	–0.4808	–18.4006	N3	–0.5036	–18.4336
Ga4	0.7721	–1.1962	Ga4	0.7743	–1.2083	Ga4	0.7180	–1.2039
Ga5	0.8091	–1.1979	Ga5	0.8119	–1.2112	Ga5	0.7652	–1.2021
Ga6	0.7606	–1.1941	Ga6	0.7669	–1.2099	Ga6	0.7306	–1.2032
N7	–0.3423	–18.4162	N7	–0.3361	–18.4004	N7	–0.3931	–18.4070
N8	–0.5688	–18.404	N8	–0.5144	–18.405	N8	–0.5123	–18.4245
N9	–0.3881	–18.4279	N9	–0.4067	–18.426	N9	–0.4522	–18.4177
N10	–0.3665	–18.4177	N10	–0.3795	–18.4173	N10	–0.44178	–18.4168
N11	–0.3514	–18.405	N11	–0.3569	–18.3885	N11	–0.4080	–18.4018
N12	–0.4238	–18.4007	N12	–0.4074	–18.3925	N12	–0.5027	–18.4131
Ga13	0.7548	–1.1592	Ga13	0.7569	–1.1935	Ga13	0.5812	–1.1741
N14	–0.4026	–18.4062	N14	–0.4192	–18.3949	N14	–0.4049	–18.3901
N15	–0.4153	–18.4014	N15	–0.4281	–18.3969	N15	–0.4072	–18.3865
$Ni^{2+}16$	0.2424	–17.6907	$Cu^{2+}16$	0.1772	–26.1028	$Zn^{2+}16$	0.9062	–22.1220

Furthermore, in Figure 3 (a-c), the electric potential amounts of NQR for some elements, including Cr^{3+}, Mn^{2+}, Co^{2+}, Ni^{2+}, Cu^{2+}, and Zn^{2+}, were assessed by the $Ga_5N_{10}Nc$ (Figure 1) through metal cation adsorption using the CAM–B3LYP/EPR–3 method and the LANL2DZ basis set.

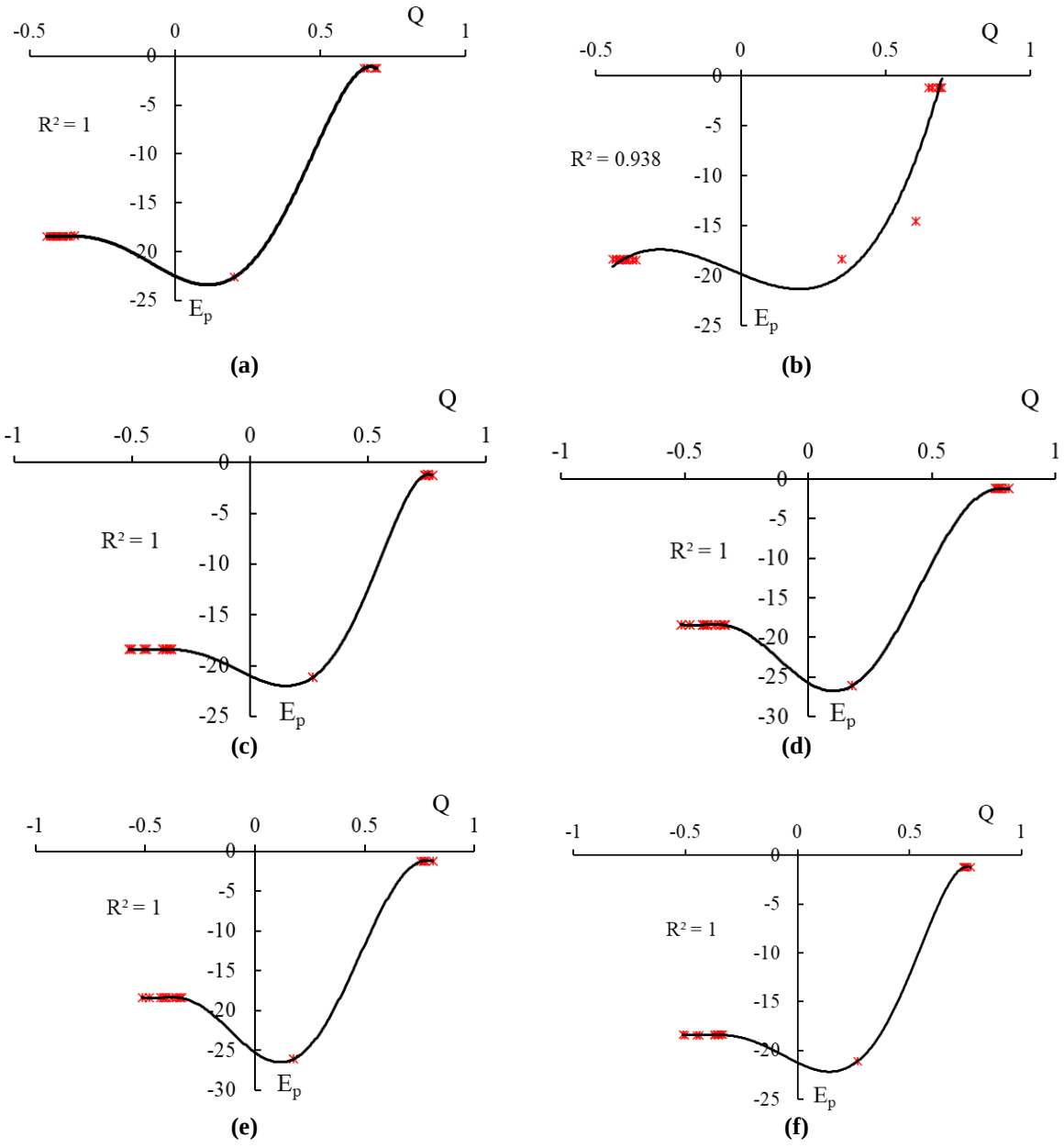

Figure 3. The amounts of electric potential (Ep/a.u.) versus Bader charge (Q/coulomb) through NQR calculation for **(a)** Cr^{3+}→ $Ga_5N_{10}Nc$; **(b)** Mn^{2+}→ $Ga_5N_{10}Nc$; **(c)** Co^{2+}→ $Ga_5N_{10}Nc$; **(d)** Ni^{2+}→ $Ga_5N_{10}Nc$; **(e)** Cu^{2+}→ $Ga_5N_{10}Nc$; **(f)** Zn^{2+}→ $Ga_5N_{10}Nc$ complexes by CAM–B3LYP/EPR–3, LANL2DZ.

In Figure 3 (a–f), the behavior of trapping of main group cations of Cr^{3+}, Mn^{2+}, Co^{2+}, Ni^{2+}, Cu^{2+}, Zn^{2+} by $Ga_5N_{10}Nc$ for sensing the water metal cations. It's clear that the graph of $Ga_5N_{10}Nc$ is twisted by these metal cations. The strongest graphs for electric potential were introduced surrounding heavy metal cations trapping on the $Ga_5N_{10}Nc$, which indicate the electron receiving specifications of these atoms vis-a-vis the gallium and nitrogen elements of $Ga_5N_{10}Nc$ (Figure 3a–f).

3.2. Analysis of NMR spectra.

Based on the resulting amounts, NMR spectrum of $Ga_5N_{10}Nc$ as the intense detector for adsorbing heavy metal cations of Cr^{3+}, Mn^{2+}, Co^{2+}, Ni^{2+}, Cu^{2+}, Zn^{2+} can unravel the efficiency of $Ga_5N_{10}Nc$ for detecting and removing of these metal cations in water toward calculating the isotropic chemical-shielding (CSI) and anisotropic chemical-shielding (CSA) [76]:

$$\sigma_{iso} = (\sigma_{11} + \sigma_{22} + \sigma_{33})/3 \quad (9)$$

$$\sigma_{aniso} = \sigma_{33} - (\sigma_{22} + \sigma_{11})/2 \quad (10)$$

The chemical shielding extracted from NMR might be employed for assigning the geometrical and structural properties of nanomaterials. In fact, the Gauge Invariant Atomic Orbital (GIAO) technique was proposed as a reliable technique for NMR measurements, and our own N-layered Integrated molecular Orbital and Molecular mechanics (ONIOM) has gained much consideration for the NMR chemical shielding of metal cation-nanocage clusters such as σ_{iso} becomes visible in equation (11):

$$\sigma_{iso,ONIOM} = \sigma_{iso,high(QM1)} + \sigma_{iso,medium(QM2)} + \sigma_{iso,low(QM3)} \quad (11)$$

The NMR quantities of isotropic (σ_{iso}) and anisotropic shielding tensor (σ_{aniso}) of Cr^{3+}, Mn^{2+}, Co^{2+}, Ni^{2+}, Cu^{2+}, Zn^{2+} trapped on the in the $Ga_5N_{10}Nc$ towards formation of Cr^{3+}→ $Ga_5N_{10}Nc$, Mn^{2+}→ $Ga_5N_{10}Nc$, Co^{2+}→ $Ga_5N_{10}Nc$, Ni^{2+}→ $Ga_5N_{10}Nc$, Cu^{2+}→ $Ga_5N_{10}Nc$, and Zn^{2+}→ $Ga_5N_{10}Nc$ complexes was carried out by Gaussian 16 revision C.01 software [68] and was announced in Table 2.

Table 2. Data of NMR shielding tensors for selected atoms of Cr^{3+}→ $Ga_5N_{10}Nc$, Mn^{2+}→ $Ga_5N_{10}Nc$, Co^{2+}→ $Ga_5N_{10}Nc$, Ni^{2+}→ $Ga_5N_{10}Nc$, Cu^{2+}→ $Ga_5N_{10}Nc$, and Zn^{2+}→ $Ga_5N_{10}Nc$ complexes using CAM-B3LYP/LANL2DZ calculation.

Cr^{3+}→ $Ga_5N_{10}Nc$			**Mn^{2+}→ $Ga_5N_{10}Nc$**			**Co^{2+}→ $Ga_5N_{10}Nc$**		
Atom	**σ_{iso}**	**σ_{aniso}**	**Atom**	**σ_{iso}**	**σ_{aniso}**	**Atom**	**σ_{iso}**	**σ_{aniso}**
Ga1	5.2765	13.2974	Ga1	11.0695	13.6433	Ga1	5.6810	18.9861
N2	94.4501	417.7068	N2	72.4403	721.6493	N2	342.1768	559.7751
N3	290.8514	563.8486	N3	61.0038	330.4238	N3	62.3018	1192.2699
Ga4	3.1441	17.3543	Ga4	7.7454	11.7636	Ga4	5.4648	11.8282
Ga5	3.4880	16.0087	Ga5	7.5412	12.5633	Ga5	4.6536	14.1755
Ga6	2.0479	13.1714	Ga6	8.3608	11.7431	Ga6	2.7077	16.7535
N7	36.8430	297.1785	N7	128.8174	664.7594	N7	709.8946	619.2750
N8	342.9284	639.8952	N8	120.1573	411.1817	N8	50.2290	767.3064
N9	150.9994	258.2649	N9	268.5831	245.4882	N9	298.9368	749.4002
N10	207.8224	328.9841	N10	318.4594	213.5165	N10	656.5956	1251.1180

Cr^{3+}→ $Ga_5N_{10}Nc$			Mn^{2+}→ $Ga_5N_{10}Nc$			Co^{2+}→ $Ga_5N_{10}Nc$		
Atom	**σ_{iso}**	**σ_{aniso}**	**Atom**	**σ_{iso}**	**σ_{aniso}**	**Atom**	**σ_{iso}**	**σ_{aniso}**
N11	112.4465	285.4540	N11	255.0156	518.3519	N11	720.5804	1097.0482
N12	96.9264	293.8636	N12	89.7359	360.1790	N12	87.9593	652.6357
Ga13	12.1237	15.8109	Ga13	16.7927	14.7687	Ga13	13.1520	56.6769
N14	428.1963	1007.0436	N14	559.6697	1381.9619	N14	544.7177	1571.2608
N15	271.1031	710.0339	N15	433.6568	1247.5613	N15	332.5274	1398.8223
Cr^{3+}16	3748.2886	1672.6447	Mn^{2+}16	4719.5776	2656.2680	Co^{2+}16	10162.7220	11019.8983
Ni^{2+}→ $Ga_5N_{10}Nc$			Cu^{2+}→ $Ga_5N_{10}Nc$			Zn^{2+}→ $Ga_5N_{10}Nc$		
Atom	**σ_{iso}**	**σ_{aniso}**	**Atom**	**σ_{iso}**	**σ_{aniso}**	**Atom**	**σ_{iso}**	**σ_{aniso}**
Ga1	649.6192	1316.3439	Ga1	0.6328	53.8739	Ga1	1.1505	15.1536
N2	349.6511	474.3277	N2	30.7673	1375.7189	N2	321.2016	791.3213
N3	99.7003	375.3947	N3	177.9079	6187.1948	N3	562.5535	1422.2608
Ga4	152.7173	2456.9387	Ga4	9.8233	40.0111	Ga4	4.0422	11.8404
Ga5	104.9527	2260.6570	Ga5	6.4564	20.6418	Ga5	2.0858	17.5502
Ga6	578.3738	1445.3685	Ga6	0.1026	32.4627	Ga6	3.8910	15.6017
N7	204.0450	296.1672	N7	490.7907	490.7907	N7	279.4842	433.9235
N8	85.2955	396.9523	N8	534.2455	6603.7421	N8	591.1636	1479.6928
N9	217.8254	372.6935	N9	605.5220	5105.7304	N9	351.5254	679.2914
N10	92.4197	356.9493	N10	2106.0979	4593.1616	N10	273.8483	879.9883
N11	162.6234	210.2113	N11	1930.6718	4839.4877	N11	334.3923	458.6278
N12	195.1064	150.7753	N12	1379.1311	4665.9490	N12	141.1314	729.3398
Ga13	923.4071	1347.2733	Ga13	38.0757	126.0629	Ga13	7.4591	13.8373
N14	79.4124	354.6668	N14	187.7882	1535.5815	N14	353.0253	1077.8138
N15	121.5089	310.7653	N15	448.3089	1521.5101	N15	413.2544	975.2774
Ni^{2+}16	6861.1725	5883.0750	Cu^{2+}16	11697.8728	16682.0809	Zn^{2+}16	698.1070	552.8403

NMR amounts in Table 2 indicated the remarkable parameters for metal cations of Cr^{3+}, Mn^{2+}, Co^{2+}, Ni^{2+}, Cu^{2+}, and Zn^{2+}, which were trapped in the $Ga_5N_{10}Nc$ as the selective sensor for detecting metal ions in water.

In fact, the encapsulation of Cr^{3+}, Mn^{2+}, Co^{2+}, Ni^{2+}, Cu^{2+}, and Zn^{2+} ions can introduce spin polarization on the (Cr^{3+}, Mn^{2+}, Co^{2+}, Ni^{2+}, Cu^{2+}, Zn^{2+})–encapsulated $Ga_5N_{10}Nc$, which indicates that these surfaces might be applied as magnetic energy storage. So, it was exhibited that the isotropic and anisotropic shielding fluctuate with the occupancy in the electron-accepting metal cations trapped in the $Ga_5N_{10}Nc$.

Figure 4 exhibited the same tendency of shielding for magnesium and aluminum, but a striking aberration from metal cations of chromium (Figure 4a), manganese (Figure 4b), cobalt (Figure 4c), nickel (Figure 4d), copper (Figure 4e), and zinc (Figure 4f) through trapping in the $Ga_5N_{10}Nc$.

In Figure4 (a–f), heavy metal cations of Cr^{3+}, Mn^{2+}, Co^{2+}, Ni^{2+}, Cu^{2+}, Zn^{2+} in the complexes of Cr^{3+}→ $Ga_5N_{10}Nc$ (Figure 4a), Mn^{2+}→ $Ga_5N_{10}Nc$ (Figure 4b), Co^{2+}→ $Ga_5N_{10}Nc$ (Figure4c), Ni^{2+}→ $Ga_5N_{10}Nc$ (Figure 4d), Cu^{2+}→ $Ga_5N_{10}Nc$ (Figure 4e), and Zn^{3+}→ $Ga_5N_{10}Nc$ (Figure4f) denote the oscillation in the chemical shielding during ion trapping.

As a matter of fact, Figure 4 (a–f) represents the gap chemical shielding between gallium/nitrogen in Ga–N nanocage and metal cations. Therefore, it might be brought up that the turnover of electron admitting for the trapped heavy metal cations in the $Ga_5N_{10}Nc$ is Ni^{2+}>>> Cu^{2+} > Co^{2+}> Mn^{2+} > Cr^{3+} >> Zn^{2+}, which indicates the potency of covalent bond across gallium/nitrogen and these heavy metal cations towards ion removal.

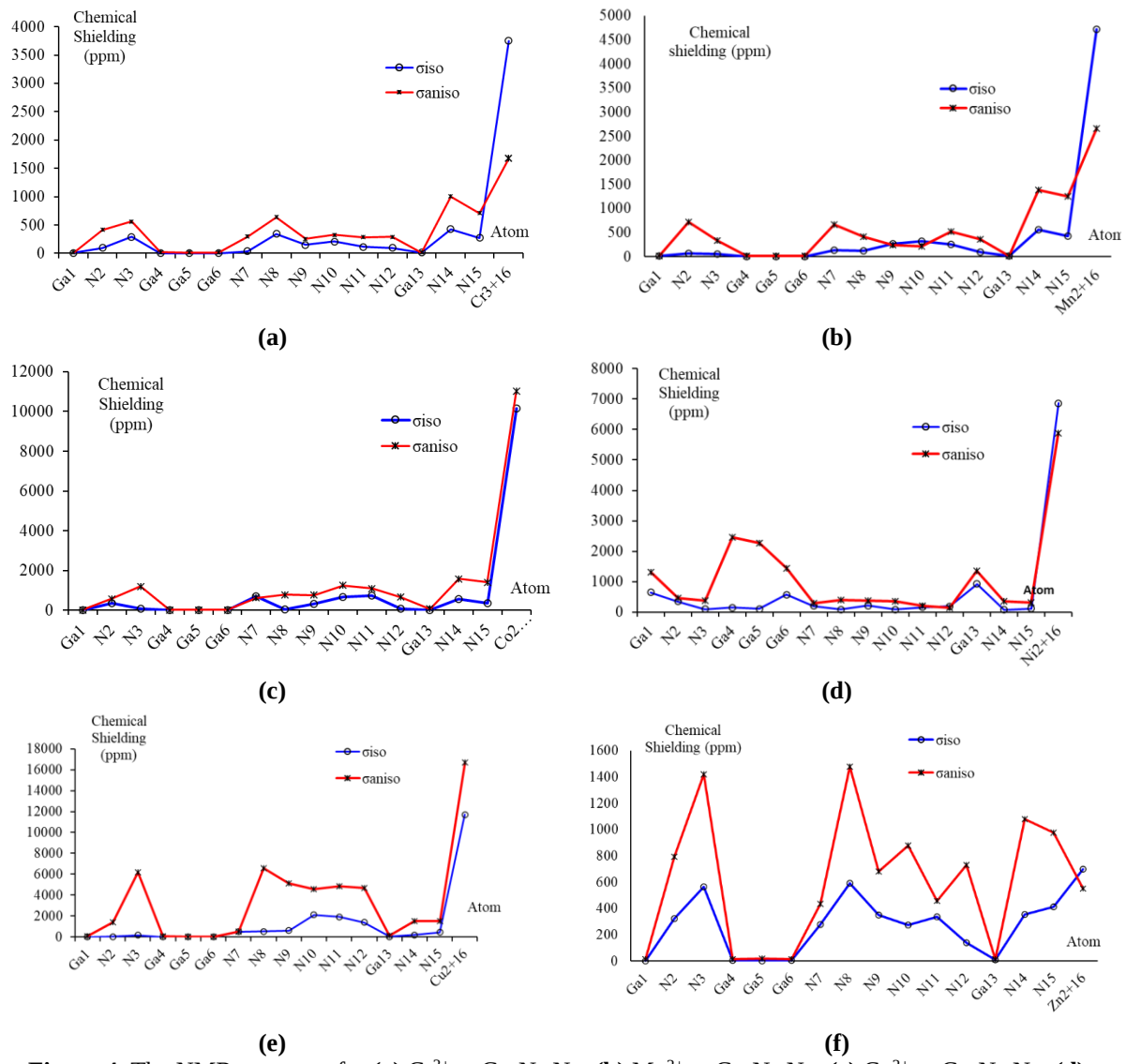

Figure 4. The NMR spectrum for **(a)** Cr^{3+}→ $Ga_5N_{10}Nc$; **(b)** Mn^{2+}→ $Ga_5N_{10}Nc$; **(c)** Co^{2+}→ $Ga_5N_{10}Nc$; **(d)** Ni^{2+}→ $Ga_5N_{10}Nc$; **(e)** Cu^{2+}→ $Ga_5N_{10}Nc$; **(f)** Zn^{2+}→ $Ga_5N_{10}Nc$ using CAM-B3LYP/LANL2DZ.

3.4. Infrared (IR) spectroscopy and thermochemical factors.

The IR calculations have been accomplished for trapping of metal cations of Cr^{3+}, Mn^{2+}, Co^{2+}, Ni^{2+}, Cu^{2+}, Zn^{2+} in the $Ga_5N_{10}Nc$ during ion sensing in water. Therefore, it has been simulated the several clusters containing Cr^{3+}→ $Ga_5N_{10}Nc$ (Figure 4a), Mn^{2+}→ $Ga_5N_{10}Nc$ (Figure 4b), Co^{2+}→ $Ga_5N_{10}Nc$ (Figure 4c), Ni^{2+}→ $Ga_5N_{10}Nc$ (Figure 4d), Cu^{2+}→ $Ga_5N_{10}Nc$ (Figure 4e), and Zn^{3+}→ $Ga_5N_{10}Nc$ (Figure 4f).

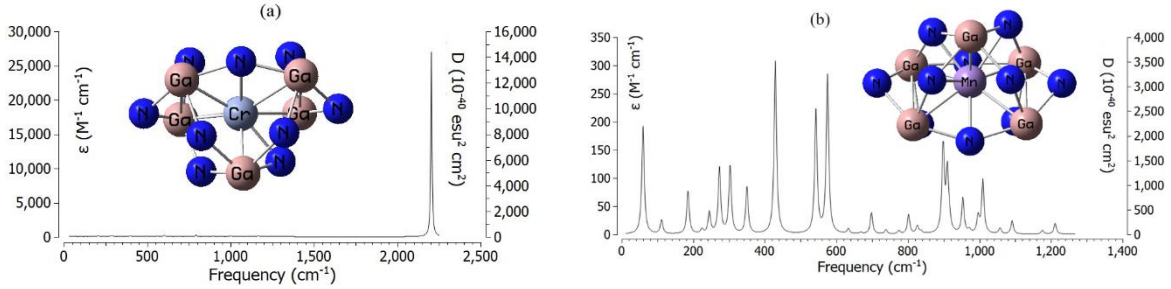

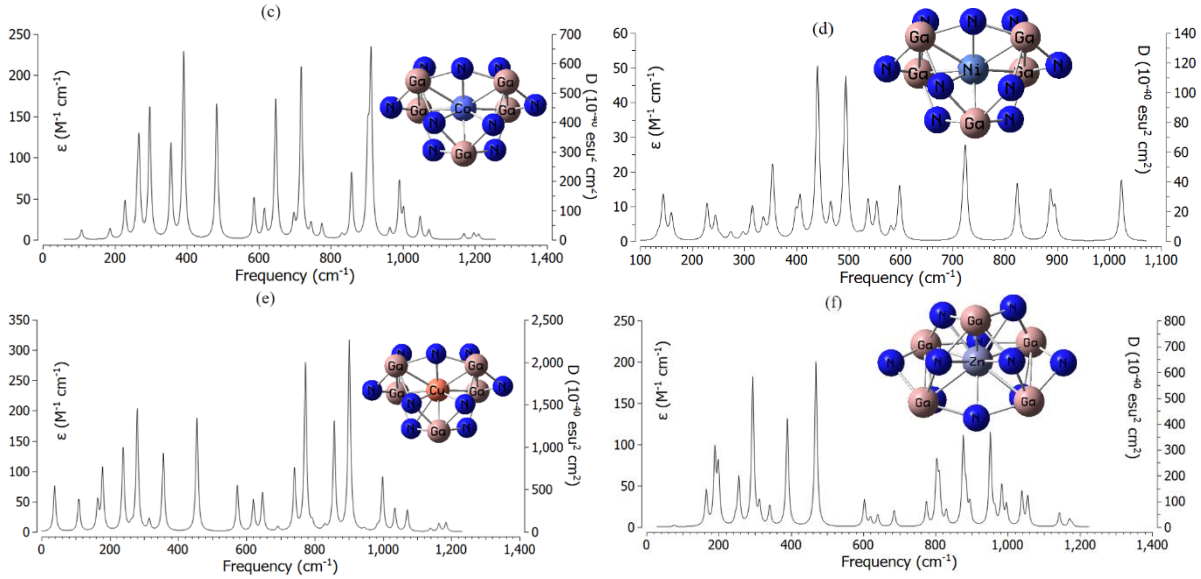

Figure 5. The Frequency (cm^{-1}) amounts of IR spectrum for **(a)** Cr^{3+}→ $Ga_5N_{10}Nc$; **(b)** Mn^{2+}→ $Ga_5N_{10}Nc$; **(c)** Co^{2+}→ $Ga_5N_{10}Nc$; **(d)** Ni^{2+}→ $Ga_5N_{10}Nc$; **(e)** Cu^{2+}→ $Ga_5N_{10}Nc$; **(f)** Zn^{2+}→ $Ga_5N_{10}Nc$ complexes.

Scientists have indicated the analysis of the intramolecular stretching band by IR spectroscopy measurements. For instance, the OH stretching was assumed into two different states of intermolecular bonding, which caused montmorillonite [Na, $Ca)_{0,3}(Al, Mg)_2Si_4O_{10}(OH)_2$ x $n(H_2O)$] to stabilize the structure of Lysozyme [77]. The curve of Figure 4 (a) was shown in the frequency limitation across 2000–2500 cm^{-1} for Cr^{3+}→ $Ga_5N_{10}Nc$ with several sharp peaks around 2204.56 cm^{-1}. Then, Figure 4 (b) was shown in the frequency limitation across 50–1200 cm^{-1} for Mn^{2+}@Ga–N_NC with several sharp peaks around 59.59, 185.25, 273.19, 302.87, 429.41, 542.86, 575.14, and 898.51 cm^{-1}. Figure 4c shows the frequency range between 100–1200 cm^{-1} for Co^{2+}→ $Ga_5N_{10}Nc$ with several sharp peaks around 296.83, 391.13, 482.89, 646.87, 717.61, and 911.57 cm^{-1}. Figure 4d shows the fluctuation of frequency between 100–1000 cm^{-1} for Ni^{2+}→ $Ga_5N_{10}Nc$ with two sharp peaks around 440.47 and 494.75 cm^{-1}. Figure 4e indicates the fluctuation of frequency between 100–1200 cm^{-1} for Cu^{2+}→ $Ga_5N_{10}Nc$ with sharp peaks around 280.23, 455.18, 772.72, 857.03, and 901.01cm^{-1}. Figure 4f shows the frequency range between 100–1200 cm^{-1} for Zn^{2+}→ $Ga_5N_{10}Nc$ with several sharp peaks around 189.25, 294.02, 468.97, and 951.76 cm^{-1}. Table 3, through the thermodynamic specifications, concluded that $Ga_5N_{10}Nc$, due to encapsulation of heavy metal cations including Cr^{3+}, Mn^{2+}, Co^{2+}, Ni^{2+}, Cu^{2+}, and Zn^{2+}, might be a more efficient sensor for detecting and removing the metal cations from water.

Table3. The thermodynamic characters of Cr^{3+}→ $Ga_5N_{10}Nc$, Mn^{2+}→ $Ga_5N_{10}Nc$, Co^{2+}→ $Ga_5N_{10}Nc$, Ni^{2+}→ $Ga_5N_{10}Nc$, Cu^{2+}→ $Ga_5N_{10}Nc$, and Zn^{2+}→ $Ga_5N_{10}Nc$ complexes using CAM-B3LYP/6-311+G (d,p), LANL2DZ calculation.

Compound	Dipole moment (Debye)	$\Delta E^o \times 10^{-3}$ (kcal/mol)	$\Delta H^o \times 10^{-3}$ (kcal/mol)	$\Delta G^o \times 10^{-3}$ (kcal/mol)	S^o (cal/K.mol)
Cr^{3+}→ $Ga_5N_{10}Nc$	1.3139	–402.912	–402.911	–402.943	105.715
Mn^{2+}→ $Ga_5N_{10}Nc$	1.0205	–413.951	–413.950	–413.981	102.154
Co^{2+}→ $Ga_5N_{10}Nc$	1.1606	–439.724	–439.723	–439.752	96.552
Ni^{2+}→ $Ga_5N_{10}Nc$	0.4812	–642.825	–642.824	–642.856	108.114
Cu^{2+}→ $Ga_5N_{10}Nc$	0.8549	–471.682	–471.682	–471.712	103.292
Zn^{2+}→ $Ga_5N_{10}Nc$	0.9645	–389.994	–389.993	–390.024	102.865

The thermodynamic data in Figure 6 could detect the maximum efficiency of metal cations (Cr^{3+}, Mn^{2+}, Co^{2+}, Ni^{2+}, Cu^{2+}, and Zn^{2+}) trapped in the $Ga_5N_{10}Nc$ through ΔG^o_{ads} which

depends on the covalent bond between heavy metal cations and $Ga_5N_{10}Nc$ as a potent sensor for water treatment.

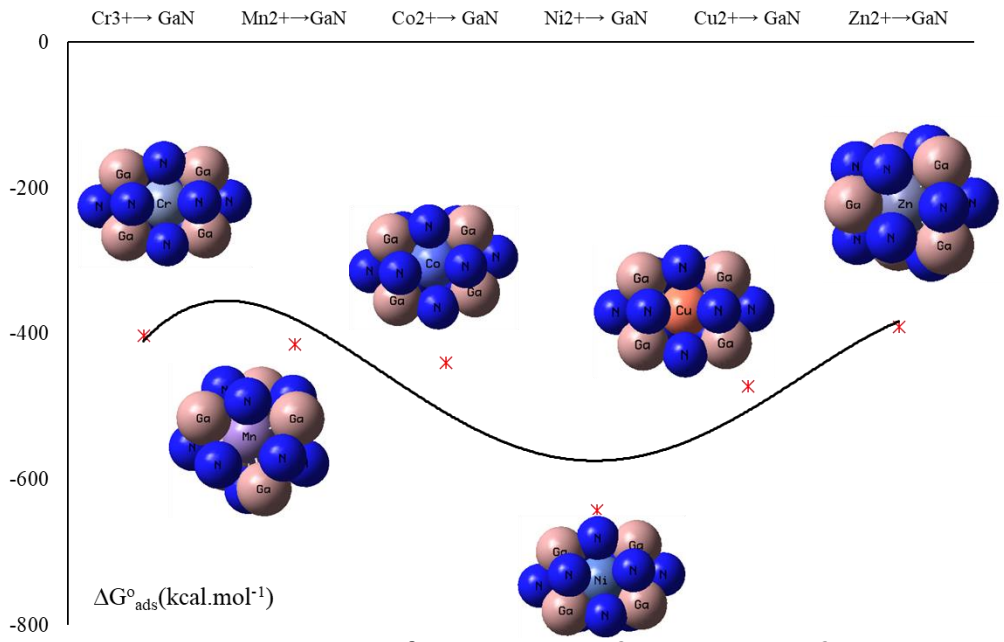

Figure 6. Gibbs free energy (ΔG^{o}_{ads}) for $Cr^{3+}\rightarrow Ga_5N_{10}Nc$, $Mn^{2+}\rightarrow Ga_5N_{10}Nc$, $Co^{2+}\rightarrow Ga_5N_{10}Nc$, $Ni^{2+}\rightarrow Ga_5N_{10}Nc$, $Cu^{2+}\rightarrow Ga_5N_{10}Nc$, and $Zn^{2+}\rightarrow Ga_5N_{10}Nc$ complexes using CAM-B3LYP/6-311+G (d,p), LANL2DZ.

The encapsulation process of metal cations including Cr^{3+}, Mn^{2+}, Co^{2+}, Ni^{2+}, Cu^{2+}, Zn^{2+} in the $Ga_5N_{10}Nc$ is affirmed by the ΔG^{o}_{ads} quantities: $\Delta G^{o}_{ads} = \Delta G^{o}_{Ions\rightarrow Ga5N10Nc} - \left(\Delta G^{o}_{Ions-grabbed} + \Delta G^{o}_{Ga5N10Nc}\right)$; Ions= Cr^{3+}, Mn^{2+}, Co^{2+}, Ni^{2+}, Cu^{2+}, Zn^{2+} (12). As seen in Table 3, all the accounted ΔG^{o}_{ads} amounts are very close.

Figure 6 shows that the dependence on the size of the ions during interaction between the adsorbates of the heavy metals cations as the electron acceptors and the adsorbent of $Ga_5N_{10}Nc$ as electron donor in the complexes of $Cr^{3+}\rightarrow Ga_5N_{10}Nc$, $Mn^{2+}\rightarrow Ga_5N_{10}Nc$, $Co^{2+}\rightarrow Ga_5N_{10}Nc$, $Ni^{2+}\rightarrow Ga_5N_{10}Nc$, $Cu^{2+}\rightarrow Ga_5N_{10}Nc$, and $Zn^{2+}\rightarrow Ga_5N_{10}Nc$ complexes. Therefore, the selectivity of metal ions by $Ga_5N_{10}Nc$ (ion sensor) can be expressed as: $Ni^{2+}>>> Cu^{2+} > Co^{2+} > Mn^{2+} > Cr^{3+} >> Zn^{2+}$ (Table 3 and Figure 6).

All in all, adsorption involving charged adsorbed species causes a change in the double layer and the potential at the outer Helmholtz plane, influencing the storage rates of both anodic and cathodic reactions. The first three modes are intimately involved in adsorption and the double layer; the last involves interaction of the heavy metal cations, trapping, and the intermediate products formed during the partial electrochemical reactions. Interaction of the adsorbed intermediates with metal cations can either decrease or increase the electrode reaction rate, depending on the stability of the metal cation-intermediate complex formed [78].

4. Conclusions

Ion separation involving a $Ga_5N_{10}Nc$ can be used to remove a series of heavy metal cations from aqueous solutions based on electrostatic interactions between the metal cations and $Ga_5N_{10}Nc$. The electromagnetic and thermodynamic properties of heavy metal cations adsorbed in the $Ga_5N_{10}Nc$ system were investigated using density functional theory. The results have illustrated that all the heavy metal cations adsorbed $Ga_5N_{10}Nc$ are rather stable, with the most stable adsorption site being in the center of the $Ga_5N_{10}Nc$ system. The adsorption of heavy

metal cations in the $Ga_5N_{10}Nc$ occurs via chemisorption. The n-trapping behavior can be found in Ga–N_NC after the adsorption of heavy metal cations. The work function of $Ga_5N_{10}Nc$ has considerably shown the heavy metals cations adsorption with maximum amount for the Ni^{2+}>>> Cu^{2+} >Co^{2+}> Cr^{3+} >> Pb^{2+} > As^{3+}–adsorbed $Ga_5N_{10}Nc$ system. In the work, we systematically investigate the stability and electronic properties of GaN monolayer under surface modification by first-principles calculation. Our results are potentially important for the fabrication of monolayer GaN-based optoelectronic devices.

Author Contributions

Conceptualization, F.M.; methodology, F.M.; data curation, F.M.; formal analysis, F.M.; investigation, F.M.; writing—original draft preparation, F.M.; writing—review and editing, F.M. All authors have read and agreed to the published version of the manuscript.

Institutional Review Board Statement

Not applicable.

Informed Consent Statement

Not applicable.

Data Availability Statement

Data supporting the findings of this study are available upon reasonable request from the corresponding author.

Funding

This research received no external funding.

Acknowledgments

In successfully completing this paper and its research, the author is grateful to Kastamonu University.

Conflict of Interest

The author declares no conflict of interest.

References

1. Lajoie, L.; Fabiano-Tixier, A.-S.; Chemat, F. Water as Green Solvent: Methods of Solubilisation and Extraction of Natural Products—Past, Present and Future Solutions. *Pharmaceuticals* **2022**, *15*, 1507, https://doi.org/10.3390/ph15121507.
2. Halleb, A.; Yokoyama, F.; das Neves, M.A.; Nakajima, M. Effects of surfactants and oil-in-water emulsions on reverse osmosis membrane performance. *Euro-Mediterr. J. Environ. Integr.* **2021**, *6*, 44, https://doi.org/10.1007/s41207-020-00236-1.
3. Cheng, Y.; Xue, F.; Yu, S.; Du, S.; Yang, Y. Subcritical Water Extraction of Natural Products. *Molecules* **2021**, *26*, 4004, https://doi.org/10.3390/molecules26134004.
4. Wang, M.; Wang, Z.; Zhang, J.; Zhan, J.; Wu, C.; Yu, W.; Fan, W.; Tang, J.; Zhang, Q.; Zhang, J. Sustainable Bioactive Salts Fully Composed of Natural Products for Enhanced Pharmaceutical

Applicability. *ACS Sustainable Chem. Eng.* **2022**, *10*, 10369–10382, https://doi.org/10.1021/acssuschemeng.2c03138.
5. Hiratsuka, A.; Yasuda, Y. Study on the Possibility of Mixed Water as a Drinking Water—From the Viewpoint of the Formation of Hydrogen-Rich Water. *J. Water Resource. Prot.* **2021**, *13*, 44–73, https://doi.org/10.4236/jwarp.2021.131004.
6. Marszałek, J.; Żyłła, R. Recovery of Water from Textile Dyeing Using Membrane Filtration Processes. *Processes* **2021**, *9*, 1833, https://doi.org/10.3390/pr9101833.
7. Alengebawy, A.; Abdelkhalek, S.T.; Qureshi, S.R.; Wang, M.-Q. Heavy Metals and Pesticides Toxicity in Agricultural Soil and Plants: Ecological Risks and Human Health Implications. *Toxics* **2021**, *9*, 42, https://doi.org/10.3390/toxics9030042.
8. Dogra, V.; Kaur, G.; Kumar, R.; Kumar, S. Toxicity profiling of metallosurfactant based ruthenium and ruthenium oxide nanoparticles towards the eukaryotic model organism *Saccharomyces cerevisiae*. *Chemosphere* **2021**, *270*, 128650, https://doi.org/10.1016/j.chemosphere.2020.128650.
9. Góralczyk-Bińkowska, A.; Długoński, A.; Bernat, P.; Długoński, J.; Jasińska, A. Environmental and molecular approach to dye industry waste degradation by the ascomycete fungus Nectriella pironii. *Sci. Rep.* **2021**, *11*, 23829, https://doi.org/10.1038/s41598-021-03446-x.
10. Wang, Y.-w.; Yi, Q.-z.; Ding, Y.; Ji, F.; Wang, N. Study on the factors influencing the dyeing performance of cotton fabric with vat dyes based on principal component analysis. *J. Text. Inst.* **2021**, *112*, 1460–1466, https://doi.org/10.1080/00405000.2020.1824432.
11. Sewu, D.D.; Lee, D.S.; Woo, S.H.; Kalderis, D. Decolorization of triarylmethane dyes, malachite green, and crystal violet, by sewage sludge biochar: Isotherm, kinetics, and adsorption mechanism comparison. *Korean J. Chem. Eng.* **2021**, *38*, 531–539, https://doi.org/10.1007/s11814-020-0727-7.
12. Singh, J.; Gupta, P.; Das, A. Dyes from Textile Industry Wastewater as Emerging Contaminants in Agricultural Fields. In Sustainable Agriculture Reviews 50: Emerging Contaminants in Agriculture, Kumar Singh, V., Singh, R., Lichtfouse, E., Eds.; Springer International Publishing: Cham, **2021**; Volume 50, pp. 109-129, https://doi.org/10.1007/978-3-030-63249-6_5.
13. Kim, B.-M.; Kim, B.; Nam, S.-E.; Eom, H.-J.; Lee, S.; Kim, K.; Rhee, J.-S. Reductive Transformation of Hexavalent Chromium in Ice Decreases Chromium Toxicity in Aquatic Animals. *Environmental Science & Technology* **2022**, *56*, 3503-3513, https://doi.org/10.1021/acs.est.1c07336.
14. Wang, Y.; Ma, J.-X.; Zhang, Y.; Xu, N.; Wang, X.-L. A Series of Cobalt-Based Coordination Polymer Crystalline Materials as Highly Sensitive Electrochemical Sensors for Detecting Trace Cr(VI), Fe(III) Ions, and Ascorbic Acid. *Cryst. Growth Des.* **2021**, *21*, 4390-4397, https://doi.org/10.1021/acs.cgd.1c00311.
15. Conour, C.S.; Droege, D.G.; Ehlke, B.; Johnstone, T.C.; Oliver, S.R.J. Selective Chromium(VI) Trapping by an Acetate-Releasing Coordination Polymer. *Inorg. Chem.* **2022**, *61*, 20824-20833, https://doi.org/10.1021/acs.inorgchem.2c03110.
16. Liu, Y.; Gan, H.; Tian, L.; Liu, Z.; Ji, Y.; Zhang, T.; Alvarez, P.J.J.; Chen, W. Partial Oxidation of FeS Nanoparticles Enhances Cr(VI) Sequestration. *Environ. Sci. Technol.* **2022**, *56*, 13954-13963, https://doi.org/10.1021/acs.est.2c02406.
17. Mollaamin, F.; Monajjemi, M. Nanomaterials for Sustainable Energy in Hydrogen-Fuel Cell: Functionalization and Characterization of Carbon Nano-Semiconductors with Silicon, Germanium, Tin or Lead through Density Functional Theory Study. *Russ. J. Phys. Chem. B.* **2024**, *18*, 607–623, https://doi.org/10.1134/S1990793124020271.
18. Gomaa, H.; Shenashen, M.A.; Elbaz, A.; Yamaguchi, H.; Abdelmottaleb, M.; El-Safty, S.A. Mesoscopic engineering materials for visual detection and selective removal of copper ions from drinking and waste water sources. *J. Hazard. Mater.* **2021**, *406*, 124314, https://doi.org/10.1016/j.jhazmat.2020.124314.
19. Bashir, F.; Irfan, M.; Ahmad, T.; Iqbal, J.; Butt, M.T.; Sadef, Y.; Umbreen, M.; Shaikh, I.A.; Moniruzzaman, M. Efficient utilization of low cost agro materials for incorporation of copper nanoparticles to scrutinize their antibacterial properties in drinking water. *Environ. Technol. Innov.* **2021**, *21*, 101228, https://doi.org/10.1016/j.eti.2020.101228.
20. Mustafa, A.; Zulfiqar, U.; Mumtaz, M.Z.; Radziemska, M.; Haider, F.U.; Holatko, J.; Hammershmiedt, T.; Naveed, M.; Ali, H.; Kintl, A.; Saeed, Q.; Kucerik, J.; Brtnicky, M. Nickel (Ni) phytotoxicity and detoxification mechanisms: A review. *Chemosphere* **2023**, *328*, 138574, https://doi.org/10.1016/j.chemosphere.2023.138574.

21. El-Naggar, A.; Ahmed, N.; Mosa, A.; Niazi, N.K.; Yousaf, B.; Sharma, A.; Sarkar, B.; Cai, Y.; Chang, S.X. Nickel in soil and water: Sources, biogeochemistry, and remediation using biochar. *J. Hazard. Mater.* **2021**, *419*, 126421, https://doi.org/10.1016/j.jhazmat.2021.126421.
22. Jain, R. Recent advances of magnetite nanomaterials to remove arsenic from water. *RSC Adv*. **2022**, *12*, 32197–32209, https://doi.org/10.1039/d2ra05832d.
23. Mollaamin, F.; Monajjemi, M. Doping of Graphene Nanostructure with Iron, Nickel and Zinc as Selective Detector for the Toxic Gas Removal: A Density Functional Theory Study. *C* **2023**, *9*, 20, https://doi.org/10.3390/c9010020.
24. Kolya, H.; Hashitsume, K.; Kang, C.-W. Recent Advances in Colorimetric Detection of Arsenic Using Metal-Based Nanoparticles. *Toxics* **2021**, *9*, 143, https://doi.org/10.3390/toxics9060143.
25. Mollaamin, F.; Mohammadi, S.; Khalaj, Z.; Monajjemi, M. Computational Modelling of Boron Nitride Nanosheet for Detecting and Trapping of Water Contaminant. *Russ. J. Phys. Chem. B.* **2024**, *18*, 67–82, https://doi.org/10.1134/S1990793124010330.
26. Velusamy, S.; Roy, A.; Sundaram, S.; Kumar Mallick, T. A Review on Heavy Metal Ions and Containing Dyes Removal Through Graphene Oxide-Based Adsorption Strategies for Textile Wastewater Treatment. *Chem. Rec.* **2021**, *21*, 1570–1610, https://doi.org/10.1002/tcr.202000153.
27. Zhang, K.; Chang, S.; Fu, Q.; Sun, X.; Fan, Y.; Zhang, M.; Tu, X.; Qadeer, A. Occurrence and risk assessment of volatile organic compounds in multiple drinking water sources in the Yangtze River Delta region, China. *Ecotoxicol. Environ. Saf.* **2021**, *225*, 112741, https://doi.org/10.1016/j.ecoenv.2021.112741.
28. Mollaamin, F.; Monajjemi, M. The influence of Sc, V, Cr, Co, Cu, Zn as ferromagnetic semiconductors implanted on B_5N_{10}-nanocarrier for enhancing of NO sensing: An environmental eco-friendly investigation. *Comput. Theor. Chem.* **2024**, *1237*, 114666, https://doi.org/10.1016/j.comptc.2024.114666.
29. Mollaamin, F. Competitive Intracellular Hydrogen-Nanocarrier Among Aluminum, Carbon, or Silicon Implantation: a Novel Technology of Eco-Friendly Energy Storage using Research Density Functional Theory. *Russ. J. Phys. Chem. B.* **2024**, *18*, 805–820, https://doi.org/10.1134/S1990793124700131.
30. Monajjemi, M.; Khaleghian, M.; Tadayonpour, N.; Mollaamin, F. THE EFFECT OF DIFFERENT SOLVENTS AND TEMPERATURES ON STABILITY OF SINGLE-WALLED CARBON NANOTUBE: A QM/MD STUDY. *Int. J. Nanosci.* **2010**, *09*, 517–529, https://doi.org/10.1142/S0219581X10007071.
31. Rudneva, I.I.; Omel'chenko, S.O. Nitrosamines in Aquatic Ecosystems: Sources, Formation, Toxicity, Environmental Risk (Review). 2. Content In Aquatic Biota, Biological Effects and Risk Assessment. *Water Resour.* **2021**, *48*, 291–299, https://doi.org/10.1134/S0097807821020135.
32. Caporossi, L.; Viganò, P.; Paci, E.; Capanna, S.; Alteri, A.; Campo, G.; Pigini, D.; De Rosa, M.; Tranfo, G.; Papaleo, B. Female Reproductive Health and Exposure to Phthalates and Bisphenol A: A Cross Sectional Study. *Toxics* **2021**, *9*, 299, https://doi.org/10.3390/toxics9110299.
33. Tripathi, S.; Sharma, P.; Singh, K.; Purchase, D.; Chandra, R. Translocation of heavy metals in medicinally important herbal plants growing on complex organometallic sludge of sugarcane molasses-based distillery waste. *Environ. Technol. Innov.* **2021**, *22*, 101434, https://doi.org/10.1016/j.eti.2021.101434.
34. Mollaamin, F.; Monajjemi, M. Electric and Magnetic Evaluation of Aluminum–Magnesium Nanoalloy Decorated with Germanium Through Heterocyclic Carbenes Adsorption: A Density Functional Theory Study. *Russ. J. Phys. Chem. B.* **2023**, *17*, 658–672, https://doi.org/10.1134/S1990793123030223.
35. Khalili Hadad, B.; Mollaamin, F.; Monajjemi, M. Biophysical chemistry of macrocycles for drug delivery: a theoretical study. *Russ. Chem. Bull.* **2011**, *60*, 238–241, https://doi.org/10.1007/s11172-011-0039-5.
36. Mollaamin, F.; Monajjemi, M. Tailoring and functionalizing the graphitic-like GaN and GaP nanostructures as selective sensors for NO, NO_2, and NH_3 adsorbing: a DFT study. *J. Mol. Model.* **2023**, 29, 170, https://doi.org/10.1007/s00894-023-05567-8.
37. Mollaamin, F. Investigating the Treatment of Transition Metals for Ameliorating the Ability of Boron Nitride for Gas Sensing & Removing: A Molecular Characterization by DFT Framework. *Prot. Met. Phys. Chem. Surf.* **2024**, *60*, 1050–1063, https://doi.org/10.1134/S2070205124702502.
38. Monajjemi, M.; Yamola, H.; Mollaamin, F. Study of Bio-nano Interaction Outlook of Amino Acids on Single-walled Carbon Nanotubes. *Fuller. Nanotub. Carbon Nanostructures* **2014**, *22*, 595–603, https://doi.org/10.1080/1536383X.2012.702163.
39. Mollaamin, F.; Monajjemi, M. Corrosion Inhibiting by Some Organic Heterocyclic Inhibitors Through Langmuir Adsorption Mechanism on the Al-X (X = Mg/Ga/Si) Alloy Surface: A Study of Quantum Three-Layer Method of CAM-DFT/ONIOM. *J. Bio-Tribo-Corros.* **2023**, *9*, 33, https://doi.org/10.1007/s40735-

023-00751-y.
40. Giannakoula, A.; Therios, I.; Chatzissavvidis, C. Effect of Lead and Copper on Photosynthetic Apparatus in Citrus (*Citrus aurantium* L.) Plants. The Role of Antioxidants in Oxidative Damage as a Response to Heavy Metal Stress. *Plants* **2021**, *10*, 155, https://doi.org/10.3390/plants10010155.
41. Mollaamin, F.; Ilkhani, A.; Sakhaei, N.; Bonsakhteh, B.; Faridchehr, A.; Tohidi, S.; Monajjemi, M. Thermodynamic and Solvent Effect on Dynamic Structures of Nano Bilayer-Cell Membrane: Hydrogen Bonding Study. *J. Comput. Theor. Nanosci*. **2015**, *12*, 3148–3154, https://doi.org/10.1166/jctn.2015.4092.
42. Feki, K.; Tounsi, S.; Mrabet, M.; Mhadhbi, H.; Brini, F. Recent advances in physiological and molecular mechanisms of heavy metal accumulation in plants. *Environ. Sci. Pollut. Res.* **2021**, *28*, 64967–64986, https://doi.org/10.1007/s11356-021-16805-y.
43. Mollaamin, F.; Monajjemi, M. Transition metal (X = Mn, Fe, Co, Ni, Cu, Zn)-doped graphene as gas sensor for CO_2 and NO_2 detection: a molecular modeling framework by DFT perspective. *J. Mol. Model.* **2023**, *29*, 119, https://doi.org/10.1007/s00894-023-05526-3.
44. Dinu, C.; Gheorghe, S.; Tenea, A.G.; Stoica, C.; Vasile, G.-G.; Popescu, R.L.; Serban, E.A.; Pascu, L.F. Toxic Metals (As, Cd, Ni, Pb) Impact in the Most Common Medicinal Plant (*Mentha piperita*). *Int. J. Environ. Res. Public Health* **2021**, *18*, 3904, https://doi.org/10.3390/ijerph18083904.
45. Mollaamin, F. Alkali Metals Doped on Tin-Silicon and Germanium-Silicon Oxides for Energy Storage in Hybrid Biofuel Cells: A First-Principles Study. *Russ. J. Phys. Chem. B.* **2025**, *19*, 720–734.
46. Tommaso, G.D.; Salvatore, M.M.; Nicoletti, R.; DellaGreca, M.; Vinale, F.; Staropoli, A.; Salvatore, F.; Lorito, M.; Iuliano, M.; Andolfi, A. Coordination Properties of the Fungal Metabolite Harzianic Acid Toward Toxic Heavy Metals. *Toxics* **2021**, *9*, 19, https://doi.org/10.3390/toxics9020019.
47. Mollaamin, F.; Monajjemi, M. Graphene-based resistant sensor decorated with Mn, Co, Cu for nitric oxide detection: Langmuir adsorption & DFT method. *Sens. Rev.* **2023**, *43*, 266–279, https://doi.org/10.1108/sr-03-2023-0040.
48. Matin, A.; Laoui, T.; Falath, W.; Farooque, M. Fouling control in reverse osmosis for water desalination & reuse: Current practices & emerging environment-friendly technologies. *Sci. Total Environ.* **2021**, *765*, 142721, https://doi.org/10.1016/j.scitotenv.2020.142721.
49. Mollaamin, F.; Monajjemi M. In Silico-DFT Investigation of Nanocluster Alloys of Al-(Mg, Ge, Sn) Coated by Nitrogen Heterocyclic Carbenes as Corrosion Inhibitors. *J. Clust. Sci.* **2023**, *34*, 2901–2918, https://doi.org/10.1007/s10876-023-02436-5.
50. AlSawaftah, N.; Abuwatfa, W.; Darwish, N.; Husseini, G. A Comprehensive Review on Membrane Fouling: Mathematical Modelling, Prediction, Diagnosis, and Mitigation. *Water* **2021**, *13*, 1327, https://doi.org/10.3390/w13091327.
51. Mollaamin, F.; Shahriari, S.; Monajjemi, M.; Khalaj, Z. Nanocluster of Aluminum Lattice via Organic Inhibitors Coating: A Study of Freundlich Adsorption. *J. Clust. Sci.* **2023**, *34*, 1547-1562, https://doi.org/10.1007/s10876-022-02335-1.
52. Mulyawan, R.; Muarif, A. A Review Of Reverse Osmosis Membrane Fouling: Formation and Control. *Int. J. Eng. Sci. Inf. Technol.* **2021**, *1*, 110–115, https://doi.org/10.52088/ijesty.v1i3.127.
53. Mollaamin, F.; Monajjemi, M. Molecular modelling framework of metal-organic clusters for conserving surfaces: Langmuir sorption through the TD-DFT/ONIOM approach. *Mol. Simul.* **2023**, *49*, 365–376, https://doi.org/10.1080/08927022.2022.2159996.
54. Ullah, A.; Tanudjaja, H.J.; Ouda, M.; Hasan, S.W.; Chew, J.W. Membrane fouling mitigation techniques for oily wastewater: A short review. *J. Water Process Eng.* **2021**, *43*, 102293, https://doi.org/10.1016/j.jwpe.2021.102293.
55. Henkelman, G.; Arnaldsson, A.; Jónsson, H. A fast and robust algorithm for Bader decomposition of charge density. *Comput. Mater. Sci.* **2006**, *36*, 354–360, https://doi.org/10.1016/j.commatsci.2005.04.010.
56. Tomasi, J.; Mennucci, B.; Cancès, E. The IEF version of the PCM solvation method: an overview of a new method addressed to study molecular solutes at the QM ab initio level. *J. Mol. Struct. THEOCHEM* **1999**, *464*, 211–226, https://doi.org/10.1016/S0166-1280(98)00553-3.
57. Frisch, M.J.; Trucks, G.W.; Schlegel, H.B.; Scuseria, G.E.; Robb, M.A.; Cheeseman, J.R.; Scalmani, G.; Barone, V.; Petersson, G.A.; Nakatsuji, H.; Li, X.; Caricato, M.; Marenich, A.V.; Bloino, J.; Janesko, B.G.; Gomperts, R.; Mennucci, B.; Hratchian, H.P.; Ortiz, J. V.; Izmaylov, A. F.; Sonnenberg, J.L.; Williams-Young, D.; Ding, F.; Lipparini, F.; Egidi, F.; Goings, J.; Peng, B.; Petrone, A.; Henderson, T.; Ranasinghe, D.; Zakrzewski, V.G.; Gao, J.; Rega, N.; Zheng, G.; Liang, W.; Hada, M.; Ehara, M.; Toyota, K.; Fukuda, R.; Hasegawa, J.; Ishida, M.; Nakajima, T.; Honda, Y.; Kitao, O.; Nakai, H.; Vreven, T.; Throssell, K.;

Montgomery, J.A., Jr.; Peralta, J.E.; Ogliaro, F.; Bearpark, M.J.; Heyd, J.J.; Brothers, E.N.; Kudin, K.N.; Staroverov, V.N.; Keith, T.A.; Kobayashi, R.; Normand, J.; Raghavachari, K.; Rendell, A.P.; Burant, J.C.; Iyengar, S.S.; Tomasi, J.; Cossi, M.; Millam, J.M.; Klene, M.; Adamo, C.; Cammi, R.; Ochterski, J.W.; Martin, R.L.; Morokuma, K.; Farkas, O.; Foresman, J.B.; Fox, D.J. Gaussian 16, Revision C.01, Gaussian, Inc., Wallingford CT, **2016**.

58. Scalmani, G.; Frisch, M.J. Continuous surface charge polarizable continuum models of solvation. I. General formalism. *J. Chem. Phys.* **2010**, *132*, 114110, https://doi.org/10.1063/1.3359469.
59. Monajjemi, M.; Karachi, N.; Mollaamin, F. The Investigation of Sequence-dependent Interaction of Messenger RNA Binding to Carbon Nanotube. *Fuller. Nanotub. Carbon Nanostructures* **2014**, *22*, 643–662, https://doi.org/10.1080/1536383X.2012.717557.
60. Perdew, J.P.; Burke, K.; Ernzerhof, M. Generalized Gradient Approximation Made Simple. *Phys. Rev. Lett.* **1996**, *77*, 3865, https://doi.org/10.1103/PhysRevLett.77.3865.
61. Mollaamin, F.; Monajjemi, M. Structural, Electromagnetic and Thermodynamic Analysis of Ion Pollutants Adsorption in Water by Gallium Nitride Nanomaterial: a Green Chemistry Application. *Russ. J. Phys. Chem. B.* **2024**, *18*, 533–548, https://doi.org/10.1134/S199079312402012X.
62. Zadeh, M.A.A.; Lari, H.; Kharghanian, L.; Balali, E.; Khadivi, R.; Yahyaei, H.; Mollaamin, F.; Monajjemi, M. Density Functional Theory Study and Anti-Cancer Properties of Shyshaq Plant: In View Point of Nano Biotechnology. *J. Comput. Theor. Nanosci.* **2015**, *12*, 4358-4367, https://doi.org/10.1166/jctn.2015.4366.
63. Hohenberg, P.; Kohn, W. Inhomogeneous Electron Gas. *Phys. Rev.* **1964**, *136*, B864, https://doi.org/10.1103/PhysRev.136.B864.
64. Kohn, W.; Sham, L.J. Self-Consistent Equations Including Exchange and Correlation Effects. *Phys. Rev.* **1965**, *140*, A1133, https://doi.org/10.1103/PhysRev.140.A1133.
65. Becke, A.D. Density-functional thermochemistry. III. The role of exact exchange. *J. Chem. Phys.* **1993**, *98*, 5648–5652, https://doi.org/10.1063/1.464913.
66. Lee, C.; Yang, W.; Parr, R.G. Development of the Colle-Salvetti correlation-energy formula into a functional of the electron density. *Phys. Rev. B* **1988**, *37*, 785, https://doi.org/10.1103/PhysRevB.37.785.
67. Mollaamin, F.; Shahriari, S.; Monajjemi, M. Influence of Transition Metals for Emergence of Energy Storage in Fuel Cells through Hydrogen Adsorption on the MgAl Surface. *Russ. J. Phys. Chem. B* **2024**, *18*, 398–418, https://doi.org/10.1134/S199079312402026X.
68. Monajjemi, M.; Noei, M.; Mollaamin, F. Design of fMet-tRNA and Calculation of its Bonding Properties by Quantum Mechanics. *Nucleos. Nucleot. Nucleic Acids* **2010**, *29*, 676–683, https://doi.org/10.1080/15257771003781642.
69. Shahriari, S.; Mollaamin, F.; Monajjemi, M. Increasing the Performance of {[(1-x-y) $LiCo_{0.3}Cu_{0.7}$] (Al and Mg doped)] O_2}, xLi_2MnO_3, $yLiCoO_2$ Composites as Cathode Material in Lithium-Ion Battery: Synthesis and Characterization. *Micromachines* **2023**, *14*, 241, https://doi.org/10.3390/mi14020241.
70. Mollaamin, F.; Monajjemi, M. Boron nitride doped with transition metals for carbon monoxide detection: a promising nanosensor for air cleaning. *Sens. Rev.* **2024**, *44*, 179–193, https://doi.org/10.1108/SR-01-2024-0066.
71. Dennington, R.; Keith, T.A.; Millam, J.M. GaussView 6.06.16. Semichem Inc., Shawnee Mission: **2016**.
72. Mollaamin, F.; Monajjemi, M. Fractal Dimension on Carbon Nanotube-Polymer Composite Materials Using Percolation Theory. *J. Comput. Theor. Nanosci.* **2012**, *9*, 597–601, https://doi.org/10.1166/jctn.2012.2067.
73. Mollaamin, F.; Monajjemi, M. In Situ Ti-Embedded SiC as Chemiresistive Nanosensor for Safety Monitoring of CO, CO_2, NO, NO_2: Molecular Modelling by Conceptual Density Functional Theory. *Russ. J. Phys. Chem. B.* **2024**, *18*, 49–66. https://doi.org/10.1134/S1990793124010159.
74. Mollaamin, F.; Monajjemi, M. Adsorption ability of Ga_5N_{10} nanomaterial for removing metal ions contamination from drinking water by DFT. *Int. J. Quantum Chem.* **2024**, *124*, e27348, https://doi.org/10.1002/qua.27348.
75. Gaidarov, M.K.; Ivanov, M.V.; Katsarov, Y.I.; Antonov, A.N. Isoscalar Giant Monopole Resonance in Spherical Nuclei as a Nuclear Matter Incompressibility Indicator. *Astronomy* **2023**, *2*, 1-13, https://doi.org/10.3390/astronomy2010001.
76. Mollaamin, F.; Monajjemi, M. Trapping of toxic heavy metals from water by GN–nanocage: Application of nanomaterials for contaminant removal technique. *J. Mol. Struct.* **2024**, *1300*, 137214, https://doi.org/10.1016/j.molstruc.2023.137214.

77. Caccamo, M.T.; Sabatino, G.; Bennardo, A.; Magazù, S. Infrared spectroscopy analysis of montmorillonite thermal effects. *IOP Conf. Ser.: Mater. Sci. Eng.* **2020**, *777*, 012002, https://doi.org/10.1088/1757-899X/777/1/012002.
78. Qasem, N.A.A.; Mohammed, R.H.; Lawal, D.U. Removal of heavy metal ions from wastewater: a comprehensive and critical review. *npj Clean Water* **2021**, *4*, 36, https://doi.org/10.1038/s41545-021-00127-0.

Publisher's Note & Disclaimer